THE JOURNAL OF PHYSICAL CHEMISTRY B

Article

pubs.acs.org/JPCB

Structural and Dynamic Features of *Candida rugosa* Lipase 1 in Water, Octane, Toluene, and Ionic Liquids BMIM-PF6 and BMIM-NO3

Patrick R. Burney and Jim Pfaendtner*

Department of Chemical Engineering, University of Washington, Seattle, Washington 98105, United States

Supporting Information

ABSTRACT: Ionic liquids (ILs) and organic chemicals can be used as solvents in biochemical reactions to influence the structural and dynamic features of the enzyme, sometimes detrimentally. In this work we report the results for molecular dynamics simulations of *Candida rugosa* lipase (CRL) in ILs BMIM-PF_6 and BMIM-NO_3, as well as organic solvents toluene and octane in an effort to explore the role of solvent on the structure and dynamics of an enzyme known to be active in many nonaqueous media. Simulations of CRL in water were also included for comparison, bringing the aggregate simulation time to over 2.8 μs. At both 310 and 375 K the ILs significantly dampen protein dynamics and trap the system near its starting structure. Structural changes in the enzyme follow the viscosity of the solvent, with the enzyme deviating from its initial structure the most in water and the least in BMIM-PF_6. Interactions between the enzyme surface and the solvent in the IL simulations show that contacts are dominated by the IL anion, which is ascribed to a broader spatial distribution of positively charged protein residues and reduced mobility of the cation due to the size of the imadazolium ring.

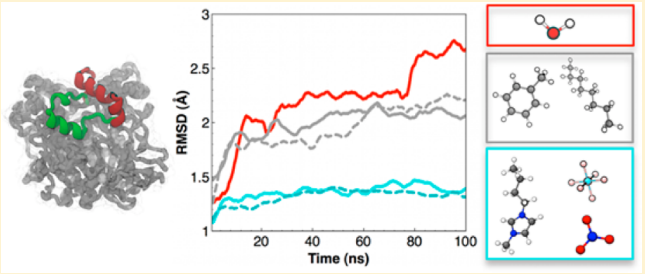

INTRODUCTION

Ionic liquids (ILs) are a novel alternative to organic solvents for many areas of chemistry. Specifically, when used as a solvent for biochemical reactions, they have the potential to add control over many reaction properties, including selectivity and product solubility. Commonly reported applications of ILs in biocatalysis include the pretreatment and catalytic breakdown of lignocellulosic biomass[1−3] and the enzymatic degradation of food waste oils.[4,5] One exciting concept regarding IL research is the wide variety of cations and anions capable of maintaining liquid phase at near-ambient conditions, providing a large library of possible solvents. It is also feasible to chemically tailor IL ions, fine-tuning atomistic functionality toward desired solvent properties.[6] Another aspect of some ILs is their ability to support enzymatic catalysis at a wide range of temperatures or concentrations of water. Not only do many enzymes retain activity in pure ILs,[7] but also they exhibit enhanced thermal stability,[8,9] selectivity,[10] and enantioselectivity[11,12] compared to traditional solvents.

Little is currently known about the molecular level change that ILs induce in an enzyme, especially those changes that lead to altered enzyme activity. The interactions between the IL and the enzyme structure may alter the equilibrium structure or dynamic fluctuations. The link between these interactions and reaction rates[13] and thermal stability remains an area of great interest. For example, *Candida rugosa*'s Lipase 1 enzyme has been shown to retain activity in the IL 1-butyl-3-methyl-imidazolium hexafluorophosphate (BMIM-PF_6) yet is rendered inactive in BMIM nitrate (BMIM-NO_3).[14] However, the current literature does little to explain how the NO_3 anion plays a role in deactivating the enzyme[14] or how BMIM-PF_6 can stabilize the enzyme at higher activity and temperatures than many other ILs.[9] The lack of experimental evidence can mostly be attributed to the inapplicability of many common experimental techniques, including in solution NMR and circular dichroism, in near-pure ionic liquids. In addition to the difficulty of purifying enzymes and the elimination of nonessential water from the solution, these limitations have restricted many studies to focus on discovery of ideal cation−anion pairs and characterizing enzyme fixation without atomistic insight guiding their search.

Molecular dynamics (MD) simulation offers an alternate way to gain molecular scale insight of the interactions between nonaqueous solvents and enzymes that to date has not been widely exploited. MD now offers access to both the dynamics and solvated structure of enzymes up to thousands of amino acids in a wide variety of solvent types at the femtosecond to microsecond time scale. Not only are these time and length scales below the limit of most experimental techniques, but also the atomic details from all-atom MD at long times scales may provide a wealth of information about cation−anion[15] and protein−ion interactions.[16,17] Applying MD simulation toward IL research may allow for simulated screening of ILs; virtually sifting through the countless anion−cation combinations toward discovering the limits of enzyme catalyzed reaction conditions and generally optimizing IL enhanced biocatalysis.

Received: December 13, 2012
Revised: January 31, 2013
Published: February 6, 2013

Several groups have spearheaded the use of simulation as a tool to investigate IL thermodynamics. Their efforts have included the first stages of developing and testing IL force fields[18,19] and have shown good accuracy when the properties of condensed phases are calculated.[20,21] Furthermore, several MD studies investigating the behavior of enzymes, including *Candida antarctica* lipase[22] and the cutinase[23] from *Fusarium solani pisi*, have explored the affect various water dilutions of ILs on ion affects at short time scales. Building from these previous works, we have completed a series of MD simulations for the purpose of investigating the affect of nonaqueous solvents on the behavior of *C. rugosa* lipase 1 (CRL).

CRL was chosen as a model system for its industrial importance—perhaps in the future with ILs—its presence in the IL-biocatalysis literature, and its wide variety of structural motifs compared to most "toy" systems. The enzyme itself consists of 535 amino acids in an alpha-beta hydrolase fold. Features of the protein include a hydrophobic core, a variety of β sheet and helix secondary structure, and a ~25 residue "lid" (highlighted in Figure 1) which covers the active site when

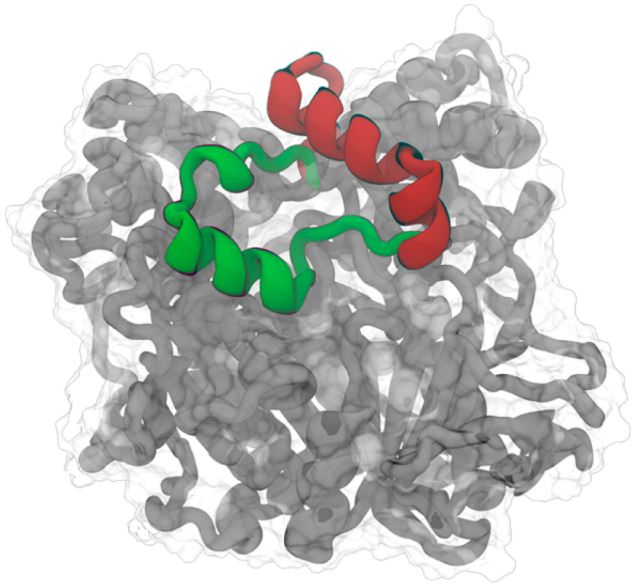

Figure 1. Two crystal structures used as the CRL initial coordinates when starting from both the open (red) and closed (green) lid conformation. The nonlid region of the structures (gray) was used for alignment.

"closed" and can spontaneously open to expose the active site's catalytic triad to the solvent. Not only does this opening transition require a proline isomerization at P92, one of the lid's hinge residues, but also the lid "bottom" and the covered portion of the active site consist primarily of hydrophobic residues. The opening transition results in a 1526 Å^2 increase in solvent-accessible surface area, of which 892 Å^2 is due to exposing hydrophobic residues.[24] These features indicate that solvation likely plays a role in the transition, which coincides with prevailing theory in the literature[25,26]—the lid-opening event is thought to occur at the presence of phase boundaries and hydrophobic environments.

Specifically, in this study we compare the influence of four nonaqueous solvents, including two ionic liquids, BMIM-PF_6 and BMIM-NO_3, and two nonpolar organic solvents, toluene and octane, on CRL at near-ambient conditions. We have also included the simulation of CRL in water for comparison. The ionic liquids BMIM-PF_6 and BMIM-NO_3 were chosen because experiments have demonstrated retained activity for CRL in BMIM-PF_6, yet no activity with the nitrate anion.[9,14] The specific mechanism of deactivation in BMIM-NO_3 has yet to be demonstrated; although other ionic liquids have been shown with FTIR or fluorescence spectroscopy to cause protein denaturation,[27,28] the case of the NO_3 anion with BMIM has not been well investigated. It is unreasonable to expect denaturation of this large of an enzyme within typical simulation time scales. For this reason we have included reference simulations at a higher temperature, 375 K, which is well above the unfolding temperature in water,[29] but not above the boiling point of our water model. This higher temperature will also serve to enhance sampling of slow protein modes for all solvents. The two nonpolar solvents were included to give contrast to both the highly charged and the highly viscous nature of the ILs. Lastly, we have completed these ten simulations (five solvents at two temperatures each) starting from both the closed (CRLC) and open (CRLO) crystal structures for a final total of twenty independent MD simulations and 2.8 μs of total simulation time.

METHODS

Model Systems. CRL exhibits the characteristic alpha/beta hydrolase fold of many hydrolase enzymes, including a HIS-SER-GLU catalytic triad and an oxyanion hole. Protein Data Bank[30] entries 1TRH[24] and 1CRL[31] were used as the initial closed and open structures, respectively, for CRL. Comparison between these two structures shows very little (<0.3 Å Cα RMSD) difference in the protein bulk and a large (17 Å Cα RMSD) variation in the lid region, residues 66−92. Aligning the two structures by the lid residues shows that lid closure is not a simple hinge-like rigid body movement and includes both rearrangement of secondary structure and a high-energy barrier in a cis−trans proline isomerization at P92.

Of the two structures, 1CRL is resolved at a higher resolution and contains 310 crystallographic waters and information of glycosylation, in the form of several *N*-acetylglucosamine (NAG), at asparagines N314 and N351. The N351 glycosylation, which contacts and forms a hydrogen bond with the lid in the CRLO crystal structure, may stabilize the lid in the open state. For this reason, the NAG residues were left intact for simulations started from the open structure and added to the closed crystal structure for the other simulations. NAG residues were parametrized with the GLYCAM06[32] force field. All structural waters were retained from the crystal structure for all simulations, including the nonaqueous simulations, as they have been shown critical toward maintaining enzyme activity.[33] De la Casa et al. have shown that lyophilized Lipase 1 contains between 220 and 522 waters per Lipase molecule.[34] Therefore, to help make connection to experiment, the surface waters from the crystal structure were also maintained, bringing the total number of water molecules in the system to 310. The water simulations were prepared by enclosing the protein in a pre-equilibrated TIP3P[35] water box using Ambertools.[36]

IL and organic solvent molecules were parametrized in antechamber[37] using GAFF force field[38] and RESP[39] partial charges after a single point Gaussian 09[40] calculation at the HF-6/31-g*(d) level of theory. Only the hexafluorophosphate from BMIM-PF_6 could not be parametrized with GAFF and the antechamber. Instead, the hexafluorophosphate molecule was

dx.doi.org/10.1021/jp312299d | J. Phys. Chem. B 2013, 117, 2662−2670

treated as rigid at the bond lengths and angles determined from a Gaussian 09 geometry optimization at the same level of theory. The force field parameters were tested against known experimental observables such as density and heat capacity (details in the Supporting Information). Initial coordinates for pure IL and organic solvent boxes, of similar dimensions to the water simulations, were generated in Packmol.[41] These boxes were equilibrated using a 5 ns *NVT* simulation at 500 K temperature followed by slowly quenching to simulation temperature and a final 10 ns *NPT* equilibration. The protein and crystallographic waters were then placed in the center of these equilibrated boxes and nonwater solvent molecules within 3.0 Å of the protein were deleted. All the simulation boxes were neutralized with counterions by replacing noncrystallographic solvent molecules. For the simulations, the number of anions and cations were equalized by random deletion of whichever were in excess. The number of atoms and the average equilibrated box size for each system is reported in the Supporting Information.

Simulation Protocol. All MD simulations and minimizations were performed using NAMD 2.7[42] and the protein was parametrized with the Amber 99SB force field.[43] First, conjugate gradient minimization was carried out with all atoms except the solvent frozen for 2000 steps, then all atoms except the protein and NAG residues were frozen for 1000 steps, and finally the entire system was mobile for another 2000 steps. The systems were then gradually heated from 0 to either 310 or 375 K using velocity rescaling *NVT* simulation to increment the temperature by 10 K every 200 ps. Production simulations were carried out in the *NPT* ensemble using the Langevin thermostat[44] and Langevin piston barostat.[45] During MD simulations a 2 fs time-step was used, the nonbonded forces were cutoff at 12 Å with a switching function starting at 11 Å, PME was used to reincorporate long-range electrostatics, and RATTLE[46] and SHAKE[47] were used to freeze hydrogen bonds. The *NPT* simulations used a dampening coefficient of 5.0 ps^{-1} for the thermostat and 200 fs for both the barostat's period and decay.

The final simulation time for all nonaqueous simulations were chosen to be 100 ns after the protein relaxed (typically occurring during the first 2−10 ns), as judged using the protein's Cα RMSD. The water simulations were taken to longer time because of the interesting behavior in the lid residues, as detailed below. The water simulations at 310 K starting from CRLO and CRLC crystal structures were taken to 600 and 250 ns, respectively, whereas at 375 K they were taken to 200 ns each. All analysis was completed with either VMD[48] or the MDAnalysis[49] package for python.

RESULTS AND DISCUSSION

Lipase Structure. Cα root mean squared deviation (RMSD) of the entire protein compared to the simulation's starting structure was used both as a measure of protein stability and as a means to monitor significant changes from the crystal structure. The lid-closed position is known to be preferred when CRL is isolated in water. On the basis of this observation, the water simulation started from the CRLC crystal structure at 310 K is considered our basis for CRL stability. The enzyme relaxes to a RMSD of about 1 Å during the first 10 ns of MD simulation, showing the enzyme backbone remains close to the initial structure upon heating. Similar behavior is seen for the 310 K simulations (Figure 2A) in the other four solvents. After 100 ns of *NPT* simulation at

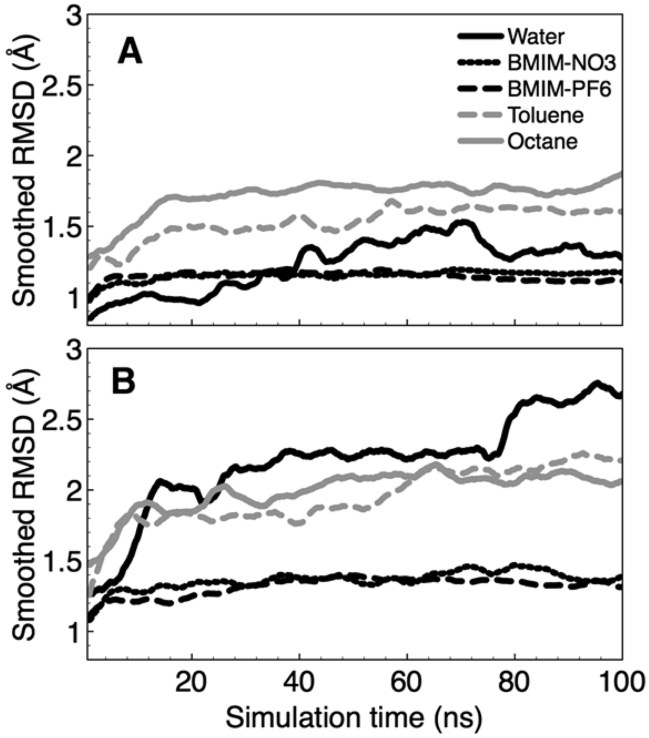

Figure 2. Smoothed Cα root mean squared deviation from the closed crystal structure for simulations started from the closed crystal structure at both 310 K (A) and 375 K (B). The raw data are not shown for clarity.

310 K, the IL and water simulations final RMSD are nearly indistinguishable at about 1 Å, whereas the two organic solvents are slightly higher, octane being the highest at close to 2 Å.

The low RMSD from simulation of other enzymes in these same ILs has been reported previously at the 10 ns time scale[23] and was concluded to be caused by "kinetic trapping". This describes how the enzyme exhibits little conformational deviation from its starting structure during any of the MD simulations. Although the simulations at high temperature show the same low RMSD (Figure 1B), the kinetic trapping previously proposed cannot be excluded as the likely cause. However, in contrast to the suggestions of Micaêlo et al.,[23] we conclude that this effect is caused by the transport properties of the ILs rather than the lack of water near the protein surface, because the surface and crystallographic waters were retained in all our simulations. Furthermore, the same behavior is also present in the IL simulations started from CRLO, indicating that the trapping is independent of exposed hydrophobic surface area and preferred native state in IL. Overall, for the chosen IL and enzyme combination we do not observe any significant structural changes on the 100 ns time scale.

In contrast to the IL simulations, the simulations in both organic solvents exhibit relaxed structures further from the initial structure and show increased RMSD at high temperature, much like the simulations in water. There are numerous characteristics that differentiate the organic and ionic liquid solvents. Among these, density, viscosity, charge and hydrogen bond participation are of particular relevance to simulation. Although experiments indicate a large decrease in viscosity for ILs at higher temperature, their viscosity is still several orders of magnitude higher than either water or the organic solvents. It is possible that the high viscosities inhibit movement away from

dx.doi.org/10.1021/jp312299d | J. Phys. Chem. B 2013, 117, 2662−2670

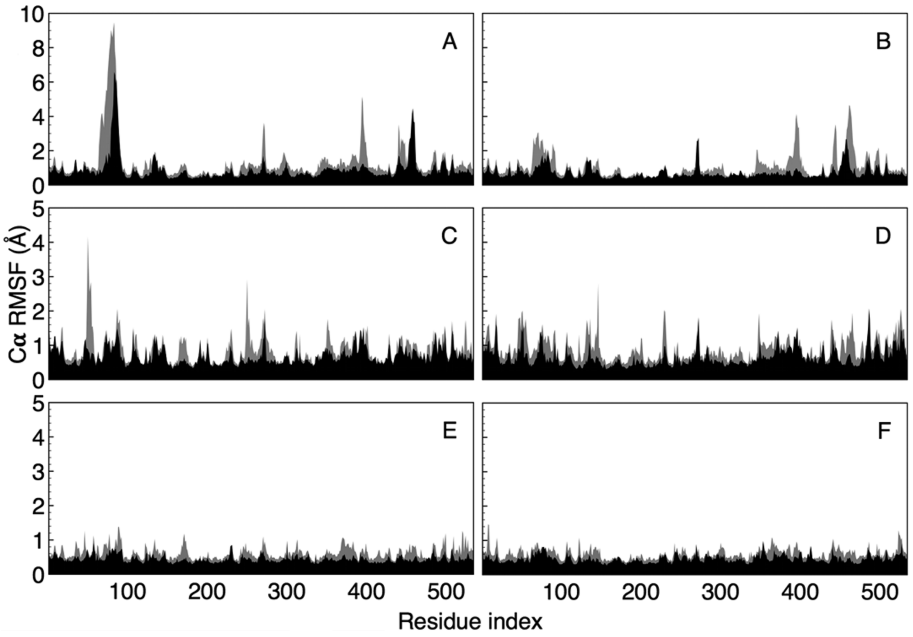

Figure 3. Cα root mean squared fluctuations of simulations started from the open (left column) and the closed (right column) crystal structure at both 310 K (black) and 375 K (gray). The water simulations (A, B) show high fluctuations in the lid and the regions of the protein that contact the lid when it is closed. In octane (C, D) these fluctuations are somewhat dampened, but in BMIM-PF6 (E, F) these fluctuations are no longer distinguishable. Note the difference in scale between row 1 and rows 2−3.

the starting structure at the simulated time scale. This effect could further be exacerbated by the anions and cations of the ionic liquid coordinating with the side chains at the enzyme surface, which will be discussed below.

Lipase Dynamics. Cα root mean squared fluctuations (RMSF), measured from the corresponding initial structure, were calculated for each trajectory after the simulations equilibrated. The systems were considered equilibrated when the RMSD leveled off after the characteristically sharp increase during the first several nanoseconds of MD simulation. For the nonaqueous simulations, this usually occurred after 2−10 ns; the aqueous simulations were judged as equilibrated after 10−20 ns, as apparent in Figure 2. To eliminate sampling as a factor when comparing simulations, each simulation was extended for at least 100 ns after equilibration. For consistency, all RMSF values and plots discussed herein are measured over the first 100 ns of simulation after equilibration.

RMSFs for the water simulations (Figure 3) reveal select regions of CRL that either underwent some rearrangement or exhibited high flexibility during the equilibrated trajectories. The largest peaks for the water simulations starting from CRLO belong to residues of the lid (residues 66−92). Even in the CRLC water simulations this region shows higher than average fluctuations, which demonstrates the highly dynamic character of the lid. Details of the lid conformational changes and dynamics will be discussed in detail below. Another region of interest for the water simulations are residues 430−475, the residues that contact the lid in CRLC and form the rim of the active site pocket. Other regions of high RMSF are the exposed random coils of surface residues 268−273 and 391−399.

In contrast to the water simulations, RMSF from simulations in the ILs (Figure 2) exhibit few pronounced features and an overall restrained movement compared to water or organic solvents. This dramatic reduction in RMSF is seen throughout the entire enzyme. Furthermore, in the IL simulations the lid region and the region surrounding the binding site are nearly indistinguishable by RMSF regardless of starting structure or simulation temperature. Although not shown here, the RMSF plots for BMIM-NO_3 are similar to those shown for BMM-PF_6—dampened and, relative to the organic or water simulations, featureless.

Results from the organic solvent simulations manifest this dampening of the lid and other regions but to a lesser degree. The RMSF for these systems also show increased fluctuations in residues 49−54, a heterogeneous patch of residues on the surface of the protein adjacent to the lid. These fluctuations are the highest in the simulation starting from CRLO in octane at 375 K, during which these residues undergo a minor conformational change which places a group of 5 polar residues into close contact and exposes a phenylalanine into the solvent.

Although the RMSF is a measure of backbone flexibility, it displays no information of side chain fluctuations. To assess the accessibly of side chain rotamers in the various solvents, we calculated the statistical entropy of the first side chain dihedral (χ_1) as $S_j = -R\sum_i P_i \ln P_i$. In this equation, S_j is the statistical entropy for residue j and P_i is the probability residue j having a χ value of i.[50] The statistical entropy of a set of values (S) is a measure of the heterogeneity of the set; a data set with values spread evenly over a wide range will show a higher value of S than a set with all the data contained in a narrow range. Extending this concept to a trajectory of side chain dihedrals results in highly flexible side chains possessing high S values whereas restricted or confined side chains show lower S values. In this case we have calculated the entropy of the χ_1 dihedral angle, which is formed by atoms N−C_α−C_β−C_γ, for residues on the surface of CRLC.

The statistical entropy for the χ_1 dihedral for all the surface residues were calculated over the first 100 ns of equilibrated trajectories for simulations started from CRLC. Using paired z-tests, the sets of entropy values for each simulation were found to be significantly different from those of the water simulation. For example, Figure 4 shows that for almost every surface

dx.doi.org/10.1021/jp312299d | J. Phys. Chem. B 2013, 117, 2662−2670

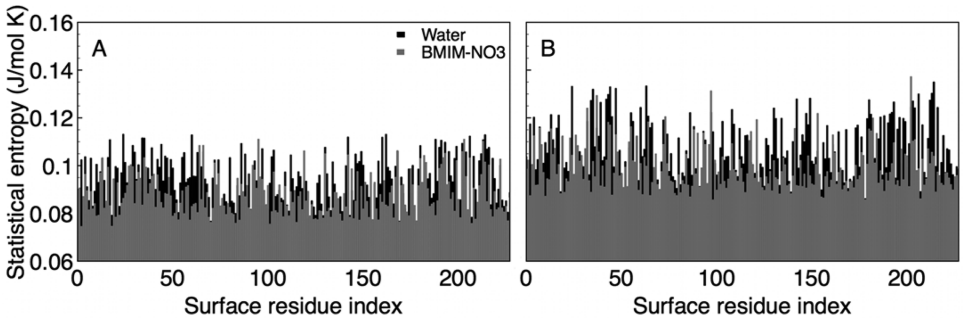

Figure 4. χ_1 statistical entropies for the surface residues of the protein are shown for both water and BMIM-NO_3 simulations started from the closed crystal structure at both 310 K (A) and 375 K (B).

residue the χ_1 entropies are higher in water than BMIM-NO_3. Further comparison between the different simulations showed that at 375 K all data sets are statistically different except when the two ILs are compared. The trend in mean entropy shows that side chain flexibility decreases as water > octane > toluene > BMIM-PF_6 > BMIM-NO_3. This series was shown to remain unchanged when only polar residues (N = 147) are considered yet changes to octane > water > toluene > BMIM-NO_3 > BMIM-PF_6 when only hydrophobic surface residues (N = 81) are considered. Considering both the lower RMSF and the decreased statistical entropy, the simulations indicate not only dampened backbone dynamics but also dampened side-chain dynamics. It is unclear whether these dampened dynamics are caused by the IL's high viscosity, coordination between the ions and amino acid residues, or some combination of these effects. The viscosity of the solvents themselves increase as octane < toluene < water < BMIM-NO_3 < BMIM-PF_6. It is interesting to note that BMIM-NO_3 has a viscosity 2 orders of magnitude higher than either water or the organic solvents, whereas BMIM-PF_6 has an even high higher viscosity than water or the organic solvents. With this consideration we might make the assumption that the difference in viscosity between water and the polar organic solvents is negligible. In this case we observe that the trend follows solvent viscosity when only hydrophobic residues are considered but not when all surface residues are considered.

Surface Behavior. With our inclusion of the 310 crystallographic surface/structural waters in the 20 simulations, we have an opportunity to examine the behavior of this water over the 100 ns time scale. Tracking the number of crystallographic waters within 4 Å of any protein atoms (Figure 5) shows a clear difference between each solvent. The water simulation shows a loss of approximately half of the initial water after the system heating, prior to *NPT* simulation. Octane and to a lesser extent toluene have the ability to trap water at the protein surface. Observing the final few nanoseconds of these simulations reveals that not only are both the water and neutralizing sodium ions staying close to the protein surface but also they are partitioned away from nonpolar residues and kept in close contact with polar side chains. This is even more apparent in the CRLO simulations due to the increased amount of exposed nonpolar surface area (Figure 6). An interesting aspect of the toluene simulations, at both low and high temperature, is that ~30 waters begin to diffuse away from the protein surface after a 39 ns lag time at 310 K and 17 ns lag time at 375 K. Compared to the octane simulations, the water and ions remaining near the protein surface are not as close to

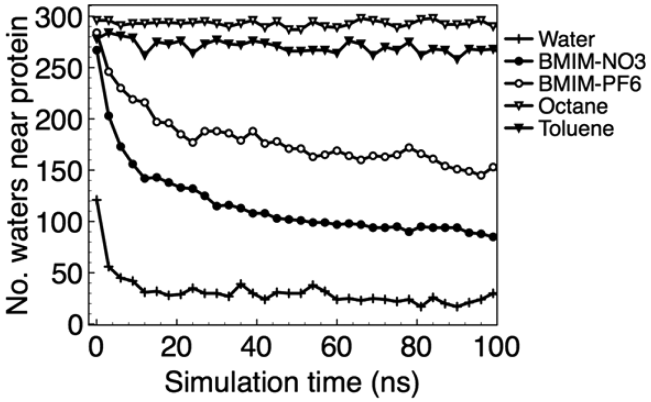

Figure 5. Number of crystallographic waters remaining within 4 Å of any protein atoms over the course of 100 ns of *NPT* simulation is plotted for the simulations starting from the closed crystal structure and at 310 K. The plot for 375 K (not shown) is almost identical.

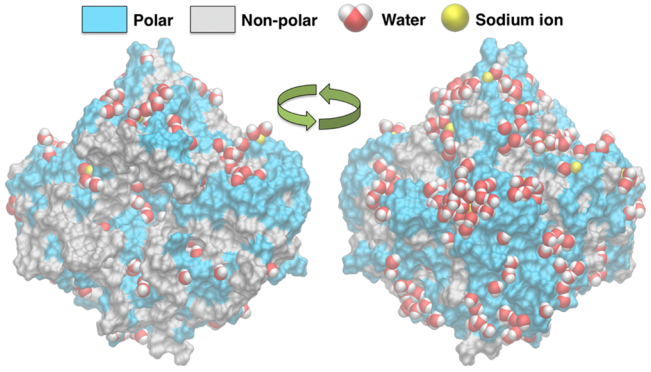

Figure 6. Snapshots of the final coordinates from the simulation started from the open crystal structure at 310 K in toluene showing that both water and sodium ions are partitioned away from hydrophobic residues. The two snapshots show the open lid face (left) and the opposite face (right) of the protein.

the protein surface although are still partitioned away from nonpolar residues.

This water/ion trapping behavior is not present in the IL simulations. This includes BMIM-PF_6, which is known to be hydrophobic and immiscible with water. As apparent in Figure 5, the IL trajectories reveal a slow and steady diffusion of water away from the protein surface. Given the apparent equal or stronger interaction of charged IL solvent with sites occupied by the crystallographic waters, one limitation to this diffusion appears to be the viscosity of ILs instead of protein−water interaction. The trend of final water count follows the trend of

dx.doi.org/10.1021/jp312299d | J. Phys. Chem. B 2013, 117, 2662−2670

viscosity and miscibility for the ILs, with BMIM-NO_3 having a much lower viscosity and greater miscibility than BMIM-PF_6. Further analysis of the IL trajectories shows that the surface waters do not exhibit the same partitioning as seen in the nonpolar solvents.

We next calculated the trajectory of contacts between protein surface residues and solvent molecules for the set of simulations at 310 K starting from CRLO. These data were sorted by residue type and residue classification (i.e., polar or nonpolar) and inspected for apparent trends. Confirming the previous analysis and the trapping effect, the data for the protein in octane shows overwhelming contact with water across all residue types. In fact, 79% of closest contacts made by the protein surface over the entire simulation are with water. When this consideration is limited by residue classification, the proportion changes to 73% for nonpolar and 83% for polar residues. Polar residues make up the majority of contacts for octane molecules, whereas sodium ions are heavily clustered around the negatively charged glutamic and aspartic acid. Comparison of the data sets for toluene and octane show that toluene can penetrate to the protein surface much more effectively than octane. Specifically, the proportion of total contacts made by water drops to 64% and the proportion of contacts made between nonpolar residues and the organic solvent molecules is 54%, compared to 24% in octane.

Applying this same analysis to the IL simulations reveals more interesting differences. For the BMIM-NO_3 system, water is replaced by the nitrate anion in making the majority of contacts with the protein surface. The most numerous contact for the nitrate anions are atoms from polar residues. Surprisingly, nitrate is able to outcompete every other solvent molecule for all contact types, including the nonpolar residues, yet not including negatively charged residues. The like−like repulsion between nitrate and negatively charged residues is enough to reduce the number of nitrate contacts to 5% for these residues. Comparison between the BMIM-PF_6 and BMIM-NO_3 simulations shows few differences. The most significant change in proportion of contacts occurs in the negatively charged residues of which the hexafluorophosphate makes up 16% of the contacts as compared to the 5% for nitrate. The BMIM-PF_6 simulations also show a slight decrease in the number of contacts between BMIM and protein surface. Because there is no apparent increase in the number of anion−protein contacts compared to that case for nitrate, it is difficult to conclude that the size of the anion is helping to exclude BMIM. The dominant coverage of the protein surface by anions may indicate that the rigidity and size of the BMIM cation restricts its ability to fill the small spaces near the side chain residues. Furthermore, anion preference at the surface may lead to stratification of the IL to avoid buildup of charge gradient in the solvent.

Lid Behavior. The increased RMSD of CRLO in water at both temperatures (not shown), and CRLC at 375 K (Figure 2B) are mostly attributable to the lid region. The lid region in all water simulations shows the most dynamic fluctuations, as seen by the RMSF in Figure 2; both simulations starting from CRLO in water exhibit the highest RMSF and RMSD of any of the 20 simulations. The RMSD of the lid residues calculated from the closed crystal structure can be used to measure closing movement for simulations started from the open crystal structure. Likewise we can calculate the lid RMSD from the open crystal structure to measure lid opening for simulations started from CRLC. On the basis of the lid RMSD (Figure 7) and visualization of the trajectory, the CRLO in water simulation at 310 K shows the lid initially opening further and making contact with another region of the enzyme bulk then undergoing some secondary structure rearrangement before closing down over the active site after ~300 ns of total simulation time.

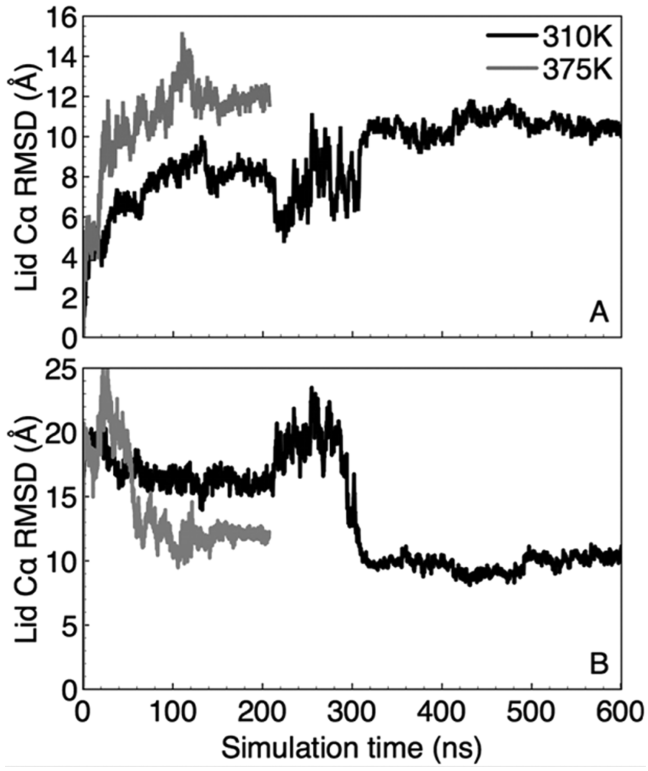

Figure 7. Cα root mean squared deviation of the lid residues compared to the open (A) and closed (B) crystal structure after aligning to the nonlid residues are shown here for simulations started from both the open crystal structures. The high temperature simulation shows similar motions on a significantly shorter time scale.

After witnessing the drastic change in RMSD, we extended this simulation to a total of 600 ns to check the stability of this new structure. Figure 7B, which shows the lid RMSD compared to CRLC for these simulations indicates that after the large closing movement around 300 ns, the lid remains stable at about 10 Å RMSD from CRLC. Viewing the final 100 ns of trajectory for this new closed state shows that there are many missing hydrophobic contacts between the lid and active site, and that although the lid makes a larger footprint on the enzyme bulk, the new closed structure only achieves partial coverage of the active site. Indeed, visualization of the trajectories allowed us to witness free transport of water molecules into and out of the active site after the lid reached this new state. Examining the trajectory of the P92 ω dihedral also reveals that the isomerization did not occur during this transition; P92 remained trans in this new closed state. These results may show that the isomerization is not a requirement for the lid to cover the binding site in water, but it is still unclear whether it is required to achieve complete active site occlusion. In addition to this 310 K closing event, another closing event occurred after only 100 ns in the 375 K simulation of CRLO in water. The final state for the higher temperature simulation is different from both CRLC and the final structure from the lower temperature. The P92 isomerization also did not occur

dx.doi.org/10.1021/jp312299d | J. Phys. Chem. B 2013, 117, 2662−2670

for this high-temperature closing event. Renderings of example frames for these closed structures have been included in the Supporting Information (Figure S1) for reference.

We stress that in addition to the bulk hinge-like movement of the lid there is a concomitant change in the lid's secondary structure, as can be seen in Figure 1, required for complete lid closure. Furthermore, the P92 trans to cis transition to move between the open and closed structure, respectively, is a major obstacle for molecular simulation due to the high energy barrier for proline isomerization (~20 kcal/mol).[51] It is has also been shown previously that the preference for either the cis or trans configuration changes with the properties of the solvent.[51] Furthermore, comparing the CRLC and CRLO structures shows an increase of 1526 Å^2 in solvent-accessible surface area upon opening, of which 892 Å^2 is due to exposing hydrophobic residues.[24] On the basis of the literature and these factors, we might have also expected an opening even in the nonpolar organic solvents. However, there was effectively no deviation in the lid configuration in any of the organic or IL simulations.

In contrast, the high temperature CRLC in water simulation did exhibit some interesting behavior (cf., Figure 2B). Visualizing the trajectory and the final structure revealed that the lid underwent some structural rearrangement and moved along the surface of the protein without opening (example structure render in Figure S1, Supporting Information). Comparing the final structure from this simulation to the other closed structures revealed it to be ~4 Å RMSD from the final structure of the CRLO in water at 375 K simulation. Visual comparison of the two structures shows remarkable similarity, with the biggest difference being in the secondary structure of a small portion and the backbone curvature near the P92 hinge, most likely caused by the difference in the ω dihedral. Considering the similarity between these structures, we have sampled an almost complete transition between the two crystal structures at 375 K. The missing components of this transition include proper placement of several hydrophobic residues and the isomerization of P92.

CONCLUSIONS

With MD we studied the affect of nonaqueous solvents on lipase 1 of *C. rugosa* at both 310 and 375 K starting from both the open and closed crystal structures. We analyzed the change in protein structure, fluctuations, the enzyme solvation, and the lid conformation. This work provides a perspective on the differences between the five solvents at the 100 ns time scale and probes aqueous conformational changes on up to the 600 ns time scale. Although we can see clear differences between the enzyme's behavior when water and the ILs are compared, at the 100 ns time scale there is little demonstrable difference between the two ILs. This observation stands despite strong experimental evidence of differences in CRL activity within these solvents and the validity of the force fields used. For the pair of ILs, it is clear that the characteristic fluctuations in the protein structure and the protein's ability to relax from its initial structure are severely reduced. There is also no evidence at this time scale of BMIM-NO3 causing the protein to denature. These observations lead us to conclude that the study of these ILs requires significantly longer sampling, which we hypothesize is due to (1) the intrinsic transport properties of the solvent and (2) the strong interactions between the protein surface and IL anions. For this reason, future MD simulation work of proteins in highly concentrated ILs would be advised to use longer simulation times or to employ some enhanced sampling methods, such as parallel tempering. Denaturing is only one of four likely mechanisms by which ILs might deactivate enzymes, the other three being inhibition by solvent molecules, covalent interactions between the IL and enzyme, and enzyme aggregation. Though the last two would be difficult to predict using MD, the first could be investigated using a substrate docking study with biased simulation such as umbrella sampling or metadynamics.

Our analysis of solvent−protein contacts demonstrates how even between two similar solvents, such as BMIM-NO3/PF6 and octane/toluene, there can be large differences in the solvation of the protein surface. The hydration (or lack thereof) of biomolecules in nonaqueous media continues to be an important point of discussion in the literature, which many researchers use to propose detailed mechanistic insights (e.g., the role of an "ice like layer of water on proteins"). Our simulations are able to discriminate subtle differences between similar solvents, and MD simulation of biomolecules in solvents using general force fields appears to be a viable way to gain qualitative insights. However, creating classical IL force fields that faithfully reproduce all structural and dynamic properties continues to be a challenge and future studies will need to couple detailed experimental observations of IL/biomolecules with simulations (e.g., coupling MD with small angle neutron scattering) to ensure quantitative accuracy.

Though it has been described in literature previously,[52,53] we have sampled several large conformational changes in the CRL lid over the course of multiple simulations. In simulations starting from the open crystal structure in water the lid closing down over the active site characterizes these conformational changes. Though these trajectories contain the lid swinging closed to the protein surface, they fail to reach the same conformation as the closed crystal structure and also do not exhibit the P92 cis−trans isomerization evident in the crystal structures. However, we can use our nearly complete lid closing trajectories to generate an initial lid-closing pathway for using path collective variable metadynamics. Results from such simulations may provide key details in the lid closing mechanism and reveal the preferred structure of the lipase lid in nonaqueous solvents.

ASSOCIATED CONTENT

Supporting Information

Details of the molecular dynamics simulations, including the number of atoms, initial and equilibrated box sizes, and the density and heat capacity of our solvent force fields. Renderings and descriptions highlighting the differences between the closed states visited in our water simulations and the closed crystal structure. This material is available free of charge via the Internet at http://pubs.acs.org.

AUTHOR INFORMATION

Corresponding Author

*E-mail: jpfaendt@u.washington.edu.

Notes

The authors declare no competing financial interest.

ACKNOWLEDGMENTS

This research was supported in part by the National Science Foundation through TeraGrid resources provided by NICS. The authors acknowledge the support of NSF award CBET-

1150596. Some MD simulations were completed using the HYAK super computer at the University of Washington.

REFERENCES

(1) Fort, D. A.; Remsing, R. C.; Swatloski, R. P.; Moyna, P.; Moyna, G.; Rogers, R. D. Can Ionic Liquids Dissolve Wood? Processing and Analysis of Lignocellulosic Materials with 1-N-Butyl-3-Methylimidazolium Chloride. *Green Chem.* **2007**, *9*, 63.

(2) Swatloski, R. P.; Spear, S. K.; Holbrey, J. D.; Rogers, R. D. Dissolution of Cellose with Ionic Liquids. *J. Am. Chem. Soc.* **2002**, *124*, 4974−4975.

(3) Binder, J. B.; Raines, R. T. Simple Chemical Transformation of Lignocellulosic Biomass into Furans for Fuels and Chemicals. *J. Am. Chem. Soc.* **2009**, *131*, 1979−1985.

(4) Ha, S. H.; Lan, M. N.; Lee, S. H.; Hwang, S. M.; Koo, Y.-M. Lipase-Catalyzed Biodiesel Production from Soybean Oil in Ionic Liquids. *Enzyme Microb. Technol.* **2007**, *41*, 480−483.

(5) Guo, Z.; Xu, X. Lipase-Catalyzed Glycerolysis of Fats and Oils in Ionic Liquids: A Further Study on the Reaction System. *Green Chem.* **2006**, *8*, 54.

(6) Carlisle, T. K.; Bara, J. E.; Gabriel, C. J.; Noble, R. D.; Gin, D. L. Interpretation of Co2 Solubility and Selectivity in Nitrile-Functionalized Room-Temperature Ionic Liquids Using a Group Contribution Approach. *Ind. Eng. Chem. Res.* **2008**, *47*, 7005−7012.

(7) Lozano, P.; de Diego, T.; Guegan, J.-P.; Vaultier, M.; Iborra, J. L. Stabilization of A-Chymotrypsin by Ionic Liquids in Transesterification Reactions. *Biotechnol. Bioeng.* **2001**, *75*, 563−569.

(8) Lozano, P.; De Diego, T.; Carrié, D.; Vaultier, M.; Iborra, J. L. Enzymatic Ester Synthesis in Ionic Liquids. *J. Mol. Catal. B: Enzym.* **2003**, *21*, 9−13.

(9) Ulbert, O.; Belafi-Bako, K.; Tonova, K.; Gubicza, L. Thermal Stability Enhancement of Candida Rugosa Lipase Using Ionic Liquids. *Biocatal. Biotransform.* **2005**, *23*, 177−183.

(10) Lozano, P.; De Diego, T.; Carrié, D.; Vaultier, M.; Iborra, J. L. Over-Stabilization of Candida Antarctica Lipase B by Ionic Liquids in Ester Synthesis. *Biotechnol. Lett.* **2001**, *23*, 1529−1533.

(11) Park, S.; Kazlauskas, R. J. Improved Preparation and Use of Room-Temperature Ionic Liquids in Lipase-Catalyzed Enantio- and Regioselective Acylations. *J. Org. Chem.* **2001**, *66*, 8395−8401.

(12) Ulbert, O.; Fráter, T.; Bélafi-Bakó, K.; Gubicza, L. Enhanced Enantioselectivity of Candida Rugosa Lipase in Ionic Liquids as Compared to Organic Solvents. *J. Mol. Catal. B: Enzym.* **2004**, *31*, 39−45.

(13) Kamerlin, S. C. L.; Warshel, A. At the Dawn of the 21st Century: Is Dynamics the Missing Link for Understanding Enzyme Catalysis? *Proteins: Struct., Funct., Bioinf.* **2010**, *78*, 1339−1375.

(14) Kaar, J. L.; Jesionowski, A. M.; Berberich, J. A.; Moulton, R.; Russell, A. J. Impact of Ionic Liquid Physical Properties on Lipase Activity and Stability. *J. Am. Chem. Soc.* **2003**, *125*, 4125−4131.

(15) Canongia Lopes, J. N. A.; Pádua, A. A. H. Nanostructural Organization in Ionic Liquids. *J. Phys. Chem. B* **2006**, *110*, 3330−3335.

(16) Curtis, R. A.; Ulrich, J.; Montaser, A.; Prausnitz, J. M.; Blanch, H. W. Protein-Protein Interactions in Concentrated Electrolyte Solutions. *Biotechnol. Bioeng.* **2002**, *79*, 367−380.

(17) Ghosh, T.; Kalra, A.; Garde, S. On the Salt-Induced Stabilization of Pair and Many-Body Hydrophobic Interactions. *J. Phys. Chem. B* **2005**, *109*, 642−651.

(18) Micaêlo, N. M.; Baptista, A. M.; Soares, C. M. Parametrization of 1-Butyl-3-Methylimidazolium Hexafluorophosphate/Nitrate Ionic Liquid for the Gromos Force Field. *J. Phys. Chem. B* **2006**, *110*, 14444−14451.

(19) Morrow, T. I.; Maginn, E. J. Molecular Dynamics Study of the Ionic Liquid 1-N-Butyl-3-Methylimidazolium Hexafluorophosphate. *J. Phys. Chem. B* **2002**, *106*, 12807−12813.

(20) Urukova, I.; Vorholz, J.; Maurer, G. Solubility of Co2, Co, and H2 in the Ionic Liquid [Bmim][Pf6] from Monte Carlo Simulations. *J. Phys. Chem. B* **2005**, *109*, 12154−12159.

(21) Maginn, E. J. Molecular Simulation of Ionic Liquids: Current Status and Future Opportunities. *J. Phys.: Condens. Matter* **2009**, *21*, 373101.

(22) Klähn, M.; Lim, G. S.; Seduraman, A.; Wu, P. On the Different Roles of Anions and Cations in the Solvation of Enzymes in Ionic Liquids. *Phys. Chem. Chem. Phys.* **2011**, *13*, 1649.

(23) Micaêlo, N. M.; Soares, C. M. Protein Structure and Dynamics in Ionic Liquids. Insights from Molecular Dynamics Simulation Studies. *J. Phys. Chem. B* **2008**, *112*, 2566−2572.

(24) Grochulski, P.; Li, Y.; Schrag, J. D.; Cygler, M. Two Conformational States of Candida Rugosa Lipase. *Protein Sci.* **1994**, *3*, 82−91.

(25) Dave, R.; Madamwar, D. Preparations for the Use of Candida Rugosa Lipase in Non-Conventional Solvents. *Biocatal. Biotransform.* **2010**, *28*, 157−166.

(26) Domínguez De María, P.; Sánchez-Montero, J. M.; Sinisterra, J. V.; Alcántara, A. R. Understanding Candida Rugosa Lipases: An Overview. *Biotechnol. Adv.* **2006**, *24*, 180−196.

(27) Madeira Lau, R.; Sorgedrager, M. J.; Carrea, G.; van Rantwijk, F.; Secundo, F.; Sheldon, R. A. Dissolution of Candida Antarctica Lipase B in Ionic Liquids: Effects on Structure and Activity. *Green Chem.* **2004**, *6*, 483.

(28) Turner, M. B.; Spear, S. K.; Huddleston, J. G.; Holbrey, J. D.; Rogers, R. D. Ionic Liquid Salt-Induced Inactivation and Unfolding of Cellulase from Trichoderma Reesei. *Green Chem.* **2003**, *5*, 443.

(29) Fuciños González, J. P.; Bassani, G.; Farruggia, B.; Picó, G. A.; Pastrana Castro, L.; Rua, M. L. Conformational Flexibility of Lipase Lip1 from Candida Rugosa Studied by Electronic Spectroscopies and Thermodynamic Approaches. *Protein J.* **2011**, *30*, 77−83.

(30) Berman, H.; Henrick, K.; Nakamura, H. Announcing the Worldwide Protein Data Bank. *Nat. Struct. Biol.* **2003**, *10*, 980.

(31) Grochulski, P.; Li, Y.; Schrag, J. D.; Bouthillier, F.; Smith, P.; Harrison, D.; Rubin, B.; Cygler, M. Insights into Interfacial Activation from an Open Structure of Candida Rugosa Lipase. *J. Biol. Chem.* **1993**, *268*, 12843−7.

(32) Kirschner, K. N.; Yongye, A. B.; Tschampel, S. M.; Gonzalez-Outeirino, J.; Daniels, C. R.; Foley, B. L.; Woods, R. J. Glycam06: A Generalizable Biomolecular Force Field. Carbohydrates. *J. Comput. Chem.* **2008**, *29*, 622−55.

(33) Levy, Y.; Onuchic, J. N. Water Mediation in Protein Folding and Molecular Recognition. *Annu. Rev. Biophys. Biomol. Struct.* **2006**, *35*, 389−415.

(34) de la Casa, R. M.; Sánchez-Montero, J. M.; Rojas, R.; Sinisterra, J. V. Simple Determination of the Water Content in Lyophilized Isoenzymes of Candida Rugosa Lipase. *Biotechnol. Tech.* **1998**, *12*, 823−827.

(35) Jorgensen, W. L.; Chandrasekhar, J.; Madura, J. D.; Impey, R. W.; Klein, M. L. Comparison of Simple Potential Functions for Simulation Liquid Water. *J. Chem. Phys.* **1983**, *79*, 926−935.

(36) Case, D. A.; Cheatham, T. E.; Darden, T.; Gohlke, H.; Luo, R.; Merz, K. M.; Onufriev, A.; Simmerling, C.; Wang, B.; Woods, R. J. The Amber Biomolecular Simulation Programs. *J. Comput. Chem.* **2005**, *26*, 1668−1688.

(37) Wang, J.; Wang, W.; Kollman, P. A.; Case, D. A. Automatic Atom Type and Bond Type Perception in Molecular Mechanical Calculations. *J. Mol. Graphics Modell.* **2006**, *25*, 247−60.

(38) Wang, J.; Wolf, R. M.; Caldwell, J. W.; Kollman, P. A.; Case, D. A. Development and Testing of a General Amber Force Field. *J. Comput. Chem.* **2004**, *25*, 1157−74.

(39) Bayly, C. I.; Cieplak, P.; Cornell, W. D.; Kollman, P. A. A Well-Behaved Electrostatic Potential Based Method Using Charge Restraints for Deriving Atomic Charges - the Resp Model. *J. Phys. Chem.* **1993**, *97*, 10269−10280.

(40) Frisch, M. J.; Trucks, G. W.; Schlegel, H. B.; Scuseria, G. E.; Robb, M. A.; Cheeseman, J. R.; Scalmani, G.; Barone, V.; Mennucci, B.; Petersson, G. A.; et al. *Gaussian 09*, Revision B.01; Gaussian, Inc.: Wallingford, CT, 2009.

(41) Martínez, L.; Andrade, R.; Birgin, E. G.; Martínez, J. M. Packmol: A Package for Building Initial Configurations for Molecular Dynamics Simulations. *J. Comput. Chem.* **2009**, *30*, 2157−2164.
(42) Phillips, J. C.; Braun, R.; Wang, W.; Gumbart, J.; Tajkhorshid, E.; Villa, E.; Chipot, C.; Skeel, R. D.; Kale, L.; Schulten, K. Scalable Molecular Dynamics with Namd. *J. Comput. Chem.* **2005**, *26*, 1781−1802.
(43) Hornak, V.; Abel, R.; Okur, A.; Strockbine, B.; Roitberg, A.; Simmerling, C. Comparison of Multiple Amber Force Fields and Development of Improved Protein Backbone Parameters. *Proteins: Struct., Funct., Bioinf.* **2006**, *65*, 712−725.
(44) Schneider, T.; Stoll, E. Molecular-Dynamics Study of a 3-Dimensional One-Component Model for Distortive Phase-Transitions. *Phys. Rev. B* **1978**, *17*, 1302−1322.
(45) Feller, S. E.; Zhang, Y. H.; Pastor, R. W.; Brooks, B. R. Constant-Pressure Molecular-Dynamics Simulation - the Langevin Piston Method. *J. Chem. Phys.* **1995**, *103*, 4613−4621.
(46) Andersen, H. C. Rattle - a Velocity Version of the Shake Algorithm for Molecular-Dynamics Caluclations. *J. Comput. Phys.* **1983**, *52*, 24−34.
(47) Krautler, V.; van Gunsteren, W. F.; Hunenberger, P. H. A Fast Shake Algorithm to Solve Distance Constraint Equations for Small Molecules in Molecular Dynamics Simulations. *J. Comput. Chem.* **2001**, *22*, 501−508.
(48) Humphrey, W.; Dalke, A.; Schulten, K. Vmd: Visual Molecular Dynamics. *J. Mol. Graphics* **1996**, *14*, 33−38.
(49) Michaud-Agrawal, N.; Denning, E. J.; Woolf, T. B.; Beckstein, O. Mdanalysis: A Toolkit for the Analysis of Molecular Dynamics Simulations. *J. Comput. Chem.* **2011**, *32*, 2319−2327.
(50) Pickett, S. D.; Sternberg, M. J. E. Empirical Scale of Side-Chain Conformational Entropy in Protein-Folding. *J. Mol. Biol.* **1993**, *231*, 825−839.
(51) Wedemeyer, W. J.; Welker, E.; Scheraga, H. A. Proline Cis−Trans Isomerization and Protein Folding. *Biochemistry* **2002**, *41*, 14637−14644.
(52) James, J. J.; Lakshmi, B. S.; Seshasayee, A. S. N.; Gautam, P. Activation of Candida Rugosa Lipase at Alkane−Aqueous Interfaces: A Molecular Dynamics Study. *FEBS Lett.* **2007**, *581*, 4377−4383.
(53) Rehm, S.; Trodler, P.; Pleiss, J. Solvent-Induced Lid Opening in Lipases: A Molecular Dynamics Study. *Protein Sci.* **2010**, *19*, 2122−2130.